

# Optimization of welding current waveform for dissimilar material with DP590 and Al5052 by Delta-spot welding process<sup>†</sup>

Ji-Sun Kim, In-Ju Kim\* and Young-Gon Kim

Green Manufacturing Process R&D Group, Korea Institute of Industrial Technology, Gwangju 500-460, Korea

(Manuscript Received September 8, 2015; Revised February 23, 2016; Accepted February 24, 2016)

## Abstract

The automotive industry has a target goal to improve fuel consumption due to restricted exhaust gas regulation. For this reason, the applicability of lightweight material, Al alloys, Mg alloys is also being expanded. In this concept, high strength steel, DP590 and light alloy, AL5052 are joined in the right place of the car body. However, it is difficult to join to steel and aluminum by conventional fusion welding. Generally, in respect to dissimilar metal joining by fusion welding, intermetallic compound layer is formed at the joint interface, hot cracking is generated. In this study, the effect of the current waveform on the mechanical characteristics and microstructure in Delta spot welding process of dissimilar metal was investigated. As results, Intermetallic compound (IMC) layer was reduced from 2.355  $\mu\text{m}$  to 1.09  $\mu\text{m}$  by using Delta spot welding process; also the welding current range improved by 50% in the delta spot welding, higher than in the inverter resistance welding. To conclude, the delta spot welding process adopting the process tapes contributes to improving the welding quality for dissimilar metals (Al5052 and DP590) due to a decrease in IMC layer.

**Keywords:** Dissimilar welding; Resistance spot welding; Current waveform; Heating model; Cooling model

## 1. Introduction

The automotive welding industry is very interested in the development of lightweight vehicles to improve fuel efficiency, safety, and motion performance. Many studies have also been conducted on the replacement of the existing steel materials with lightweight aluminum and plastic materials [1, 2]. Aluminum has a better weight-lightening effect than high-tension steel, and absorbs impact better than general steel. It also has good castability, processability, and recyclability, so it is widely used as a car material. High-priced cars generally have an all-aluminum alloy body to lighten their weight, but there is an effort to achieve light weight and high body strength using not only aluminum alloy but also high-strength steel.

As mentioned, weight lightening is achieved not merely by changing the thickness and strength of an existing material, but by combining a lightweight material with a high-strength material. Accordingly, a dissimilar material bonding technique is required. In particular, aluminum and DP steel are the most widely used materials, and their usage is expected to grow continuously [3]. However, there are many problems in the fusion welding of aluminum and steel. Because each of them

does not dissolve in the other, and because they have different chemical and physical characteristics (melting point, thermal expansion coefficient, thermal conductivity, etc.), a fragile Intermetallic phase (IMP) appears at the welding boundary [4]. In the Fe-Al two-component system, only a low percentage of the aluminum becomes solid in the steel. Aluminum is a single phase of  $\alpha\text{Fe}$  ( $\text{Fe}_2\text{Al}$ ) when the aluminum is 33% or lower. When the aluminum is approximately 62%, intermetallic compounds such as  $\text{FeAl}_2$ ,  $\text{Fe}_2\text{Al}_5$ , and  $\text{FeAl}_3$  appear [5].

According to many reports, 33-62% of Al in Fe will form a fragile intermetallic compound, which can lead to cracks during the cooling of the compound after its solidification [6, 7]. Fusion welding and resistance spot welding, including arc welding, may generate an excessive Intermetallic compound (IMC) layer at the boundary, and may decrease the welding strength and the ductility [8, 9]. Nevertheless, despite the difficulty of joining steel and aluminum through the fusion state process, many studies have been conducted on this topic using conventional welding processes such as arc welding, resistance spot welding, and laser welding [10, 11]. Few studies related to Resistance spot welding (RSW) of aluminum alloy and steel have been reported that coat the Zn layer to base material is necessary to obtain the welding quality [12-14]. Most of the aforementioned studies examined the effects of the intermetallic compound on the welding performance in the case of the Al-steel dissimilar welding, and explained the gen-

\*Corresponding author. Tel.: +82 626006300, Fax.: +82 626006099

E-mail address: k9inu@kitech.re.kr

<sup>†</sup>Recommended by Associate Editor Hyung Wook Park

© KSME & Springer 2016

eration mechanism for the intermetallic compound.

In this study, we used delta spot welding, a new resistance spot welding process, to determine the differences between the general resistance spot welding and the dissimilar metal welding, and to optimize the welding process.

## 2. Materials and experimental procedure

### 2.1 Materials

The Al material used in this study was the Al-Mg series, Al5052 material (2.5% Mg), which is used for construction, cars, ships, bridges, guardrails, and low-temperature liquid gas equipment. DP590 is the most widely used AHSS in the industrial field. It is a dual-phase steel with martensite and ferrite, which has excellent strength and formability. Table 1 shows the mechanical characteristics of the Al alloy and the DP steel. The melting point of Al is lower than that of steel (approximately 1500°C). The Al-Mg series has a 570–660°C melting point. In addition, Al requires a very large quantity of heat for melting because it has high specific heat and latent heat as shown in Table 1. Its thermal conductivity is three-times higher than that of steel. Accordingly, the welding of Al requires rapid application of a large quantity of heat, and the welding must be performed rapidly with a large amount of energy. In the case of resistance welding, the electric resistance of Al is one-fourth of that of steel, and it requires a much higher power capacity than does steel. DP steel has a tissue of martensite in the form of an island in the second phase in the ferrite matrix. AHSS is defined as steel with a  $TS \times EI$  value lower than 2500 MPa%, to which category DP steel also belongs. Soft ferrite generally provides ductility to steel, and hard ferrite, strength. When steel is deformed due to an external force, the deformation is first concentrated on the soft ferrite, and then work hardening occurs from the martensite, thus showing an excellent mechanical characteristic. Accordingly, it has a higher tensile strength than steel with a similar yield strength. The weldability of DP steel is better than that of other AHSS because of its lower C content.

The demand for the two aforementioned materials is increasing in the automotive industry, and studies are underway on the method of bonding the two materials. The joining of the metals with different physical characteristics via welding is called ‘dissimilar welding’, which has two types. One type is the welding of different series (e.g., Inconel + STS), and the other type is dissimilar welding (aluminum + steel). Welding is possible in the first type if the difference between the melting points of the two metals is 100°C or less, and related studies focused on ensuring the weldability.

In the second type, however, the differences in the solubility and the melting point of the two metals determine the success of the welding. The solid solubility of the aluminum and steel in this study was almost zero. The welding test was conducted using materials that are unfeasible for general fusion welding due to their intermetallic compound.

In this study, 1.4 mm-thick AL5052 sheets and 1.5 mm-

Table 1. Mechanical characteristics of the Al5052 alloy and the DP 590.

Mechanical properties		
	DP590	Al5052
Tensile strength, ultimate	600 - 700 MPa	190 - 200 MPa
Tensile strength, yield	330 - 410 MPa	90 - 100 MPa
Elongation	$\geq 28\%$	$\geq 27\%$
Melting point	1,536°C	660.1°C
Hardness (Hv)	450	80
Thermal conductivity	38 $\Omega$ /m.K	238 $\Omega$ /m.K
Specific resistance	15.9 $\mu\Omega$ cm	2.6 $\mu\Omega$ cm

thick DP590 sheets were used. The test was followed by the welding zone fracture test, the nugget measurement, and the welding zone strength measurement to evaluate the weldability.

### 2.2 Delta-spot welding process

The delta spot welding system differs from the general resistance spot welding system in that it has a thin metal, which is called a ‘‘process tape’’, inserted between the base material and the electrode. General resistance welding applies a large current under a pressure to obtain the heat from the contact resistance and the metal resistivity occurring on the metal contact surfaces, so the metals are joined by the applied pressure when they are heated or melted. Resistance heating is the basis of all forms of resistance welding, and is essential for the process development, electrode control, or quality control in the field. The heat quantity generated when the current flows into the metal with a resistance, that is, the resistance heat  $Q$ , is expressed as follows:

$$Q = I^2 R t (J) = (\rho \delta)^2 V t (J) \quad (1)$$

where  $I$  is the current (A),  $R$  is the resistance ( $\Omega$ ),  $t$  is the welding time (seconds),  $\rho$  is the resistivity ( $\Omega$ -cm),  $V$  is the volume of the conductor, and  $\delta$  is the current density ( $I/\text{cm}^2$ ). The resistance heating for welding increases as follows. The delta spot welding system increases the number of resistant areas on the welding base material and can achieve the additional heat input effect.

Fig. 1 shows the resistance distributions for general resistance spot welding and delta spot welding. General resistance spot welding has the resistivity of the electrode ( $R_{ei}$ ), the contact resistance between the electrode and the base material ( $R_{es}$ ), the resistivity of the base material ( $R_m$ ), and the contact resistance between the base materials ( $R_{ms}$ ), as shown in Fig. 1(a). Thus, the heating effect is highest on the contact resistance surface of the base material. However, delta spot welding additionally has the contact resistance between the electrode and the process tape ( $R_{ep}$ ), the resistivity of the process tape ( $R_p$ ), and the contact resistance between the process tape and the base material ( $R_{ps}$ ), because of the insertion of the

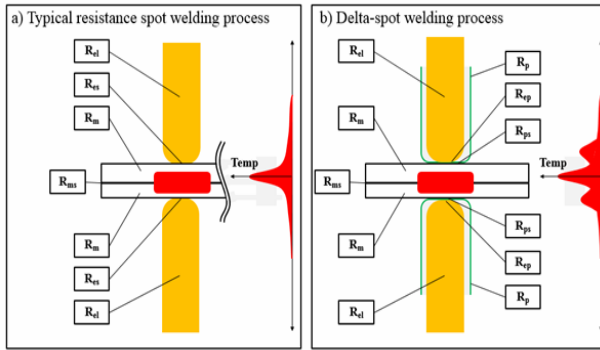


Fig. 1. Distribution of resistance in (a) typical resistance spot welding; (b) delta-spot welding process test.

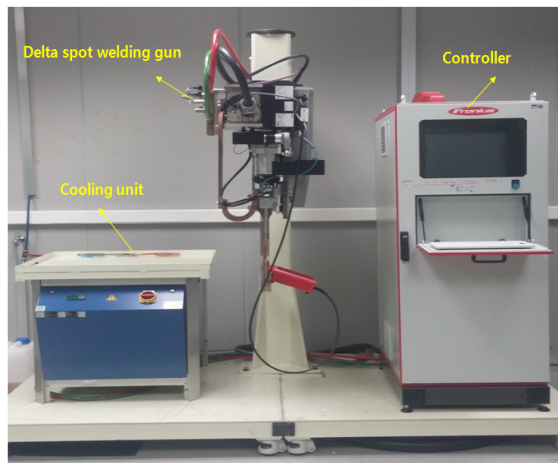


Fig. 2. Delta-spot welding systems employed in the experiment.

process tape as shown in Fig. 1(b). An increase in the entire resistance widens the heating area, and the heating position can be controlled by the type of process tape. The process tape has mainly three advantages: (1) Additional resistance heat, (2) prevention of the electrode contamination, and (3) prevention of spatters. The welding of aluminum requires a high-current welding power source because of the high thermal conductivity and low resistance of the base material, but delta spot welding can provide an excellent heating effect with the same power. Fig. 2 indicate the welding equipment used in this study. The delta spot welding system can supply an up to 36 kA current and an 8kN compressive force. The electrode had a plate-type Cr-Cu tip, and its diameter was 12 mm.

### 2.3 Experiment procedure

The welding condition for the delta spot welding experiment was a multi-pulse model, in accordance with the ISO 18278-2 standard [11], which is the typical resistance welding condition for the advanced high-strength steel standardized by a European car maker. In this study, initial welding condition waveform based on ISO 18278-2 was determined because there is no standard for dissimilar welding conditions. Nor-

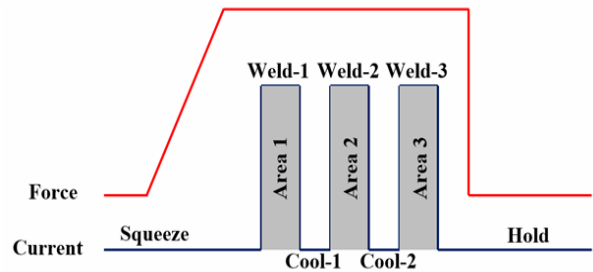


Fig. 3. Conventional spot welding waveform based on the ISO standard (steel, 1.4 mm thickness) without of process tapes.

mally, cycle time has been in used instead of welding time for spot welding process, and it is calculated by frequency of power supply. A cycle time used in this study is 16 ms because frequency of power supply employed was 60 Hz.

Fig. 3 shows the three-stage current waveform based on ISO 18278-2 when the sheet thickness is 1.4 mm. The system includes the squeezed part that fixes and stabilizes the welding material, the welded part (areas 1-3) that supplies the current, the cooling part that suppresses the temperature increase in the melted area by cutting the current, and the holding part where the melted area is stabilized after the welding. The pressure condition was set at 4.5 kN. The following four types of welding tests using delta spot welding were performed in this study, as follows:

- (1) A test to determine the weldability according to the insertion of the process tape using the current condition (11.5 kA) chosen as the suitable welding range from the typical resistance welding process test and the three-stage current waveform model.
- (2) A weldability evaluation test according to the multi-pulse heating model using the process tape determined in the first test.
- (3) A weldability evaluation test according to the cooling time rate using the heating model determined in the second test.
- (4) A lobe curve obtained by optimizing the welding condition with respect to the current and welding forces using the selected current waveform included process tape, heating model and cooling.

After each welding test, a cross-tension test was performed to measure the mechanical strength, the fracture shape, and the nugget diameter in the welding area. The fracture shape was observed and the nugget size was measured. Based on the results, the welding conditions were determined. The nugget of a single material is generally measured using a specimen with a fractured plug or by observing the melted area after the specimen is broken [15]. However, this test handles dissimilar materials with uncertain melted areas, and the fracture shape is rarely a complete plug fracture. Therefore, the nugget diameter was measured to estimate the area before the corona bond. The measurement was conducted using the averages of the two dimensions in the vertical and horizontal directions, as

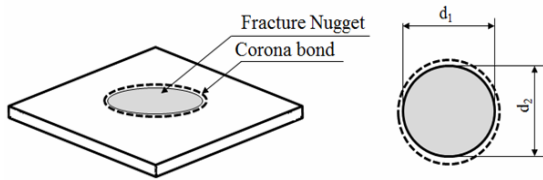


Fig. 4. Measuring method of fracture nugget diameter.

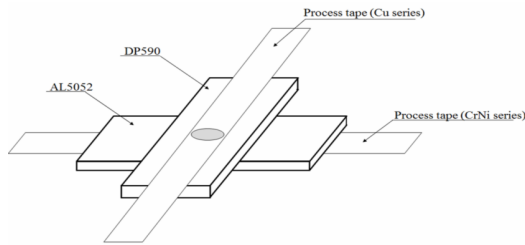


Fig. 5. Schematic description of the experiment set-up for selection of process tape.

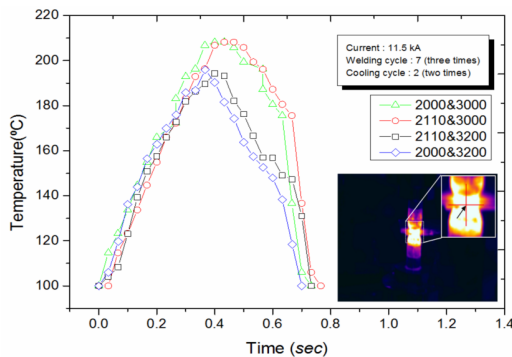


Fig. 6. Temperature profile for dissimilar welding Al5052 and DP590 according to combination of process tape.

shown in Fig. 4.

SEM was used to measure the welding area so as to analyze the fractured cross-section area and the intermetallic compound, and EDS was used to analyze the welding area. In addition, an infrared imaging camera was used to evaluate the thermal record of joint neighborhoods.

### 3. Optimization of the welding conditions

#### 3.1 Effect of the process tapes

As mentioned in Sec. 2.2, a thin sheet, called a “process tape”, was inserted to between the base metal and electrode tip. The process tape based Cu was used for the DP590 surface, and the process tape based CrNi was used for the Al5052 surface as shows in Fig. 5. The test was conducted by combining four kinds of process tapes.

Seven types of process tapes were supplied by Fronius and subdivided according to the type of their base material. The process tapes that apply to high-strength steel and aluminum are the Cu and CrNi tapes, which are each subdivided into two types according to their properties. No. 2000 and No. 2110 are

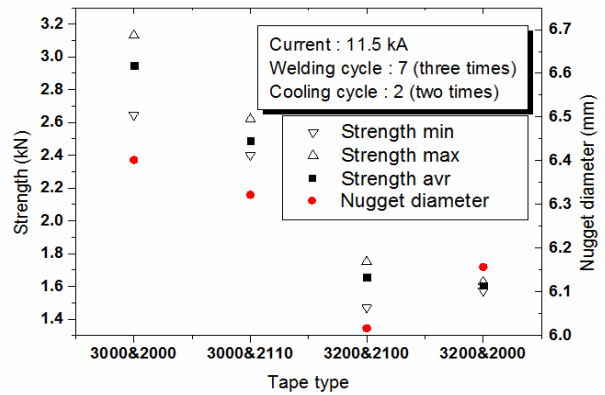


Fig. 7. Variations of cross tensile strength and nugget diameters according to combination of process tape.

Cu-based alloys that contain at least 70% Cu. No. 2110 has a 10% higher carbon content than No. 2000. No. 3000 has a Fe base and a Ni base. No. 3200 has a Fe content that is one-tenth of that of No. 3000, and is close to pure nickel alloy.

The temperature record, mechanical strength and nugget diameter in the welding area were measured according to the process tape combination. To measure the temperature profile at the welding area (the Al surface), thermo-graphic camera (FLIRT-640) was used. Thermo-graphic camera was focused on center between two electrode-tips for estimation of the melting zone temperature as shown Fig. 6.

In Fig. 6, the combination of CrNi 2000 and Cu 3000, and the combination of CrNi 2100 and Cu 3000, showed nearly 10% higher temperature records than other combinations. This means that heat input varies in the same welding condition according to the combination of the process tapes. In conclusion, a higher heat input is applied to the welding area overall when CrNi 3000 is used. Fe accounts for at least 70% of CrNi 3000, and the resistivity of Fe is  $12.299 \times 10^{-6} \Omega \text{ cm}$ . Because the resistivity of CrNi 3200 is  $7.811 \times 10^{-6} \Omega \text{ cm}$ , wherein Ni accounts for at least 80%, the difference between their resistivity values is more than two-fold. That is why the maximum temperature varies depending on which of the two process tapes is used.

As shown in the cross-tension test results and the nugget diameter in Fig. 7, the combination of CrNi 2000 and Cu 3000 had greater values than other combinations. The combination of CrNi 2000 and Cu 3000 seemingly ensured a high strength and a sufficient nugget diameter in the welding area because they had higher temperature records than other combinations. For the combination CrNi2000 and Cu3200, nugget diameter was higher than the combination CrNi2100 and Cu3200. However, welding strength was quite the opposite. It is because that a large amount of interface fracture indicated at welding specimen with combination CrNi2000 and Cu3200 than CrNi2100 and Cu3200 specimen.

In this test, it was verified that the combination of CrNi 2000 and Cu 3000 was optimal in ensuring sufficient strength and nugget diameter in the welding area in the case of the

Table 2. Characteristics of heating models.

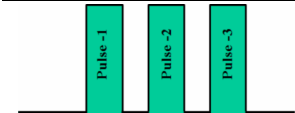
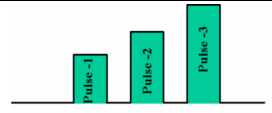
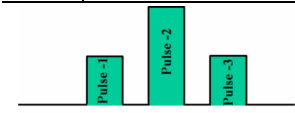
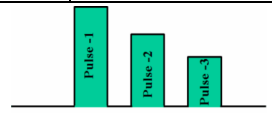
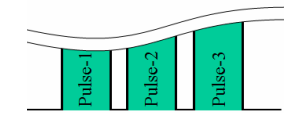
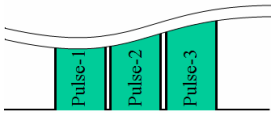
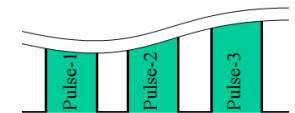
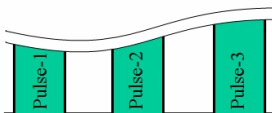
Characteristics of heating models							
No.1	Normal heating			No.2	Pre-heating		
							
Distribution of heating energy			Distribution of heating energy				
Pulse 1	Pulse 2	Pulse 3	Pulse 1	Pulse 2	Pulse 3		
33.3%	33.3%	33.3%	20%	30%	50%		
No.3	Middle-heating			No.4	Post-heating		
							
Distribution of heating energy			Distribution of heating energy				
Pulse 1	Pulse 2	Pulse 3	Pulse 1	Pulse 2	Pulse 3		
25%	50%	25%	50%	30%	20%		

Table 3. Characteristics of cooling models.

Characteristics of cooling models							
No.1	Normal-cooling			No.2	Short-cooling		
							
Cooling time(ms)			Cooling time(ms)				
1st	2nd	Cooling rate	1st	2nd	Cooling rate		
35	35	20%	16	16	9.5%		
No.3	Middle-cooling			No.4	Long-cooling		
							
Cooling time(ms)			Cooling time(ms)				
1st	2nd	Cooling rate	1st	2nd	Cooling rate		
66	66	38%	166	166	95%		

dissimilar welding of DP590 and A15052. In the next test, CrNi 2000 and Cu 3000, which were chosen in the test, were used.

### 3.2 Effect of the heating model

To determine the heating model, four heat input models were designed, as shown in Table 2. To examine the weldability according to the heating model, the total quantity of electricity was fixed at 4025 (c; coulomb), and the design test was conducted with four types of three-stage pulses.

The heat inputs of the four heat input models were the same, and the following formulas were used to calculate the heat input.

$$E = I \times t \tag{2}$$

$$PCn = E \cdot CRn. \tag{3}$$

In Eqs. (2) and (3),  $E$  is the quantity of electricity, calculated using the formula current ( $I$ ) x time ( $t$ ),  $PCn$  is the current quantity of each pulse, and  $CRn$  is the current supply rate of each pulse.

According to the ISO standard, the welding current is 11.5 kA, and the total welding time is 0.35s. The basic welding condition includes an 11.5 kA current and a 0.35s welding time, as in the process selection test in Sec. 3.1. With the total current quantity fixed at 4025 (c), the current quantity of the first, second, and third pulses was changed in the welding test, and Nugget diameters (ND) and CTS cross tensile strength (CTS) evaluations were conducted. The features of the heating models and current application methods are as follows:

(1) Normal heating model: The same current quantity is supplied three times.

(2) Pre-heating model: A low current is applied at the start of the welding to pre-heat the welding area, and 50% of the total current quantity is supplied at the third and final pulse.

(3) Middle-heating model: The greatest current quantity is supplied at the second pulse.

(4) Post-heating model: The greatest current quantity is supplied at the first pulse, and the current quantity is gradually reduced.

Three tests were conducted with each heating model, and the resulting shear tensile strength and nugget diameter measurements are shown in Fig. 8. The shear tensile strength was highest in the pre-heating model. The post-heating model had a much lower shear strength than the other models. The nugget diameters of the models were generally similar. All the models had about 6 mm nugget diameters. The nugget diameter is generally proportional to the shear strength, but in the case of the dissimilar welding, the strength of the welding area varied according to the intermetallic compound in the welding area and the solubility, even though a sufficient nugget diameter was secured. The test results showed that the shear strength of the resistance spot welding area varied according to the type of heat input model even at the same total current quantity.

### 3.3 Effect of the cooling model

The test was organized to determine the cooling model as shown in Table 3. The cooling model refers to the suspension of the current between the three-stage current pulses, and the test was conducted with current suspensions of 9.5%, 20%, 38% and 95% of the current supply time. To determine the cooling time of the heat input model, the following test was planned. The welding time of the chosen pre-heating model was 0.35 s, and three models were established by determining the cooling times of 9.5%, 20% and 95% of the welding cycle to compare the model with the existing normal cooling model.



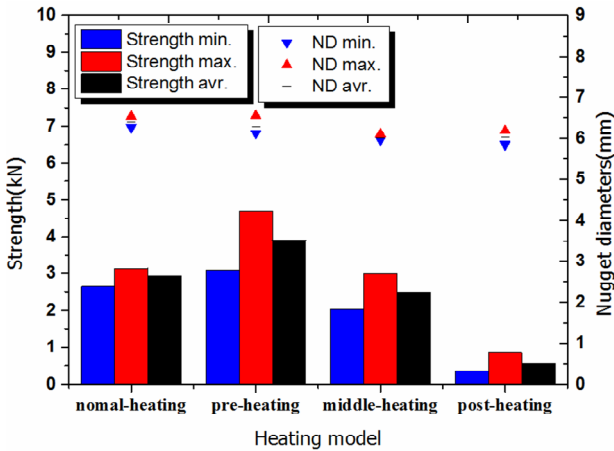


Fig. 8. Variations of cross tensile strength and nugget diameters according to heating models.

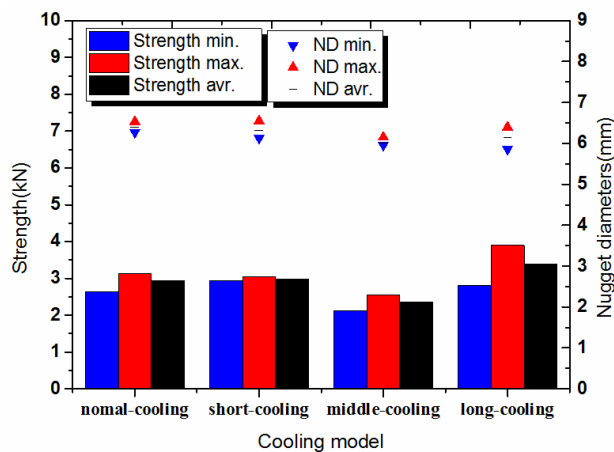


Fig. 9. Variations of cross tensile strength and nugget diameters according to cooling models.

In the existing normal cooling model, the cooling time is 20% (70 ms) of the 0.35s welding time. The three models are called the ‘short-cooling model’ (with a 9.5% cooling rate), the ‘middle-cooling model’ (with a 20% cooling rate) and the ‘long-cooling model’ (with a 95% cooling rate). The shear tensile strength and the nugget diameter of the four cooling models were evaluated as shown in Fig. 9. The long-cooling model had a shear tensile strength of 3.4 kN, which was up to 30% higher than that of the other models. It also had a 6.4 mm average nugget diameter, which was the greatest. At a cooling rate range of 9.5-20%, the shear tensile strength was approximately 2.9 kN. The nugget diameter slightly decreased within the cooling rate range of 9.5-38%, but abruptly increased at a cooling rate of 95%.

### 3.4 Drawing the lobe curve

Finally, the determined current waveform was used to conduct a welding test so as to determine the lobe curve. With the chosen pulse model, the current quantity of the first pulse is

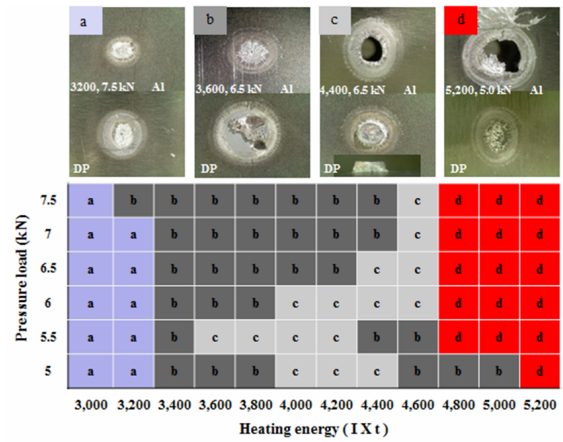


Fig. 10. Weldability lobe in Al5052 and DP950 with fracture type: (a) Interfacial fracture; (b) partial interfacial fracture; (c) plug fracture; (d) scattering.

20% of the total current quantity; of the middle pulse, 30%; and of the final pulse, 50%. The long-cooling condition was used for the cooling time. The three-stage pulse current waveform was tested by varying the total current quantity instead of using the general current quantity change. The test was conducted by increasing the current quantity from 3200 (c) to 5200 (c) with 200 (c) increments, and the pressure was increased from 5 kN to 7.5 kN with 0.5 kN increments. Each test was conducted until a welding fault occurred. Thereafter, a cross-tension test was conducted, and the fractured test specimen was used to measure the nugget diameter. At a fixed total current quantity, the current quantity of each pulse was calculated as follows Eq. (4).

$$Current = \frac{Energy \times heatingrate}{weldingtime \times 100} \tag{4}$$

As shown in Fig. 10, 72 tests were conducted, and the results were presented by type of fracture. In Fig. 10, Fig. 10(a) is an interfacial fracture wherein the melting is poor, due to which it cannot be used as a welding condition; Fig. 10(b) is a partial interfacial fracture wherein part of the aluminum is attached to DP590 steel; Fig. 10(c) is a plug fracture, the optimal fracture; and Fig. 10(d) is a welding condition that cannot ensure the strength because of the scattering in the melting area. In conclusion, range Fig. 10(c) is the most stable welding condition for AL5052 and DP590 because of its strength. Due to the welding force, the widest plug fracture was formed at 5.5-6.0 kN.

### 3.5 Effect of the welding force

Shear strength characteristic according to the welding force, the cross-tensile strength and the nugget diameter in the plug fracture area in Fig. 11 were comparatively analyzed. In the resistance spot welding between Al5052 and DP590, the in-

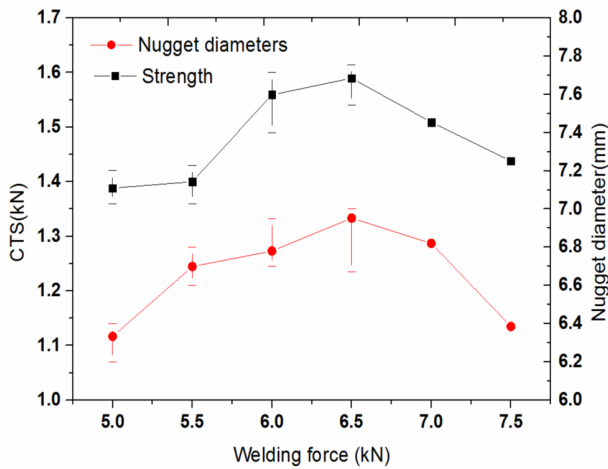
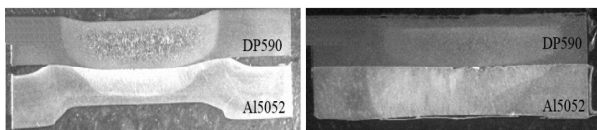


Fig. 11. Variations of cross tensile strength and nugget diameters according to welding force.



(a) Typical resistance spot welding (b) Delta-spot welding

Fig. 12. Micro images of cross section in weld zone.

termetallic compound in the welding area had diverse forms. As shown in Fig. 13 the intermetallic compound on the DP590 surface after the fracture was  $Fe_3Al$ , and the fracture progressed according to the solidification behavior of the base material. Dendrites were observed in most of the fracture surfaces, and the occurrence of brittle intermetallic compound fractures was not verified.

**3.6 Intermetallic compound (IMC) in dissimilar welding**

Difference between general spot welding and delta spot welding was observed through a Fig. 12. The cross-sectional welding area of the aluminum/steel dissimilar welding, which was performed using the general resistance spot welding technique, had a cup shape, as shown in Fig. 12(a). Melting zone was observed at center of DP590 due to higher specific resistance of material rather than contact resistance between the two materials. And heat by specific resistance was delivered to Al 5052 surface. However, as shown in Fig. 12(b), the melting zone was concentrated between the two base materials, and the melting shape appeared at the center. It is sufficient evidence for the fact that delta-spot welding process using process tape can control the melting location.

To examine the fracture characteristic of the welding area, the surface of the fractured welding area was analyzed. After the cross-tensile strength test, the surface was observed via SEM and EDS to examine the effects of the intermetallic compound on the fracture. Fig. 13(a) shows the SEM image of the aluminum welding area, and Fig. 13(b) shows the welding

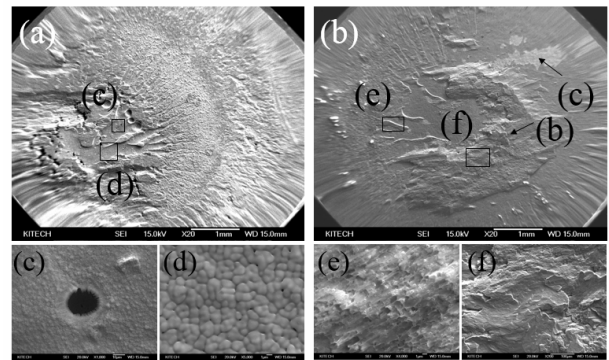


Fig. 13. SEM images of the fractured weld zone Al5052(a), DP590(b) with 11.5kA; (c), (d), (e) and (f) higher magnification view of the weld; (c) welding voids, (d) dendrites, (e) ductile fracture characteristics (fine dimple), (f) cleavage fracture characteristics.

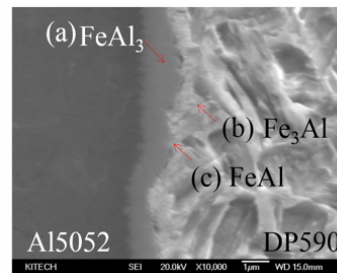


Fig. 14. SEM images and results of the EDS analysis of Intermetallic compound layer in dissimilar weld with Al5052 and DP590.

fracture of DP590. In Fig. 13(a), the fracture progressed from the center of the melting area to the right side, with dendrites formed at the center. This indicates that the dendrites, the solidified tissue of aluminum, grew vertically from the melting area. The current flowed, the center of the welding area melted, the entire area melted, and the solidification started from the center of the welding area. In addition, as shown in images Figs. 13(e) and (f), cleavage fracture and ductile fracture progressed simultaneously. The center of the welding area tended to have cleavage fractures, whereas the farther area tended to have ductile fractures.

In the resistance spot welding between Al5052 and DP590, the intermetallic compound in the welding area had diverse forms. As shown in Fig. 14 the intermetallic compound on the DP590 surface after the fracture was  $Fe_3Al$ , and the fracture progressed according to the solidification behavior of the base material. Dendrites were observed in most of the fracture surfaces, and the occurrence of brittle intermetallic compound fractures was not verified.

Figs. 15(b) and (d) show a pure aluminum base material (AL5052), and Fig. 15(c) shows  $Fe_3Al$  intermetallic compound with a 4:1 composition ratio.  $Fe_3Al$  is classified as Fe-rich intermetallic compound, and is ductile with a 250-350HV hardness. The aluminum base material remained over the intermetallic compound layer, and Fig. 15(e) showed that in the HAZ area, far from the welding center, aluminum oxide

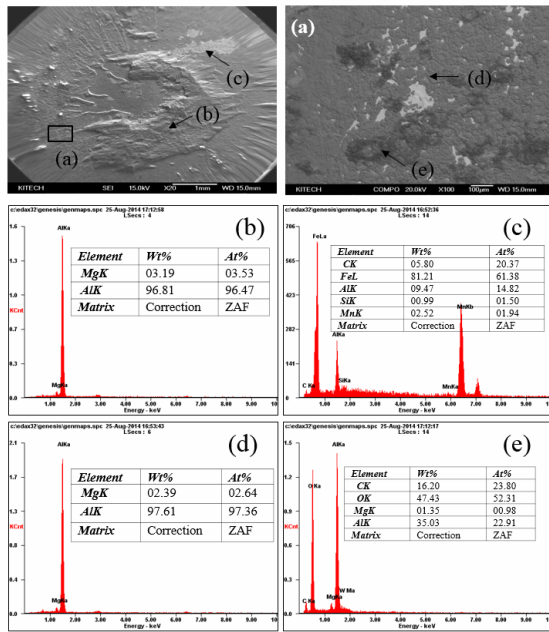


Fig. 15. SEM images and results of the EDS analysis of the surface fractured weld zone.

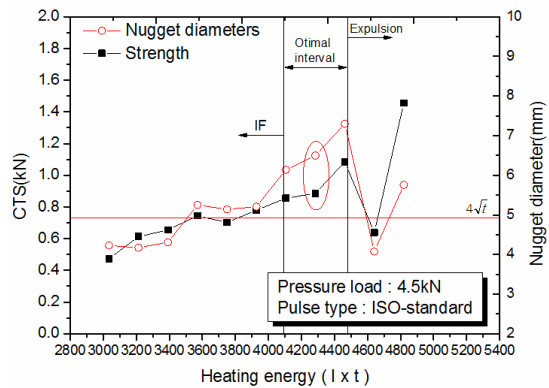


Fig. 16. Optimal welding boundary of typical inverter resistant welding process using the ISO-standard current waveform.

(Al<sub>2</sub>O<sub>3</sub>) was found.

### 3.7 Comparison between typical resistance welding and Delta-spot welding

Figs. 17 and 18 compare the existing inverter resistance welding and delta spot welding, which is an additional heat input resistance spot welding process. The proper welding conditions for each welding process are: (1) No cleavage fracture, (2) no scattering and (3) a sufficient nugget diameter.

The welding conditions were considered proper when the aforementioned conditions were met. As shown in the results, the welding current range improved by 50% in the delta spot welding, higher than in the inverter resistance welding. In the inverter resistance welding, the proper heating energy range was 4100–4500 (C), and in the delta spot welding, the current

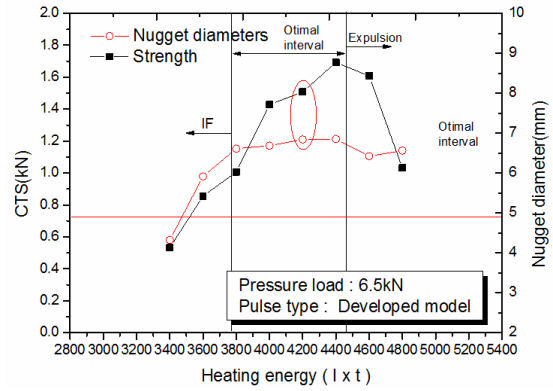


Fig. 17. Optimal welding boundary of Delta-spot welding process using the using the developed current waveform.

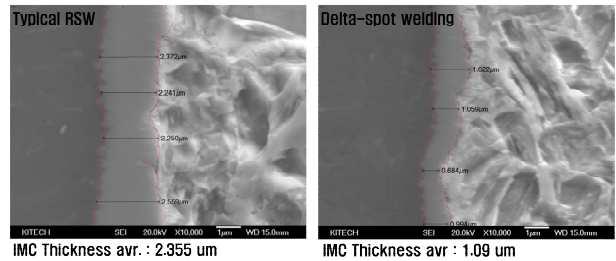


Fig. 18. Comparison IMC thickness of typical RSW and Delta-spot welding.

range widened by about 200 (c) to 4000–4600 (c). The cross-tensile strength improved by 64% in the delta-spot welding with the optimized welding condition (developed current waveform), higher than in the inverter resistance welding. The average cross-tensile strength in the proper welding range was about 0.94 kN in the inverter welding and 1.55 kN in the delta-spot welding.

In the inverter resistance welding, a 2.355 μm-thick intermetallic compound layer was formed, and in the delta spot welding, a 1.09 μm-thick intermetallic compound layer as shown Fig. 18. These were seemingly because of the increase in the strength of the welding area. They proved that the additional heat input reduced the intermetallic compound layer.

### 4. Conclusions

This research was concentrated on the developed resistance spot welding condition that can improve the welding strength and quality for dissimilar metal using the Delta-spot welding process. In addition, a new current waveform including the optimum heating and cooling models have been developed to reduce the IMC thickness. Within this research, the following conclusions have been reached.

Delta-spot welding has been applied for dissimilar welding between Al5052 and DP590. Current waveform and times of cooling and heating are chosen as input parameters to compare the welding strength and quality. The suggested new current waveform contributes to improving the welding



strength, 64% increase than typical resistance spot welding process. Intermetallic compound layer was reduced from 2.355  $\mu\text{m}$  to 1.09  $\mu\text{m}$  by using process tape and optimal wave-form developed.

## References

- [1] P. K. Mallick, *Materials, design and manufacturing for lightweight vehicles*, Woodhead Publishing, Michigan, USA (2010).
- [2] Y. G. Kim, I. J. Kim, J. S. Kim, Y. I. Chung and D. Y. Choi, Evaluation of surface crack in resistance spot welds of Zn-coated steel, *Materials Transactions*, 55 (1) (2014) 171-175.
- [3] G. Belingardi, A. T. Beyene, E. G. Koricho and B. Martorana, Alternative lightweight materials and component manufacturing technologies for vehicle frontal bumper beam, *Composite Structures*, 120 (2015) 483-495.
- [4] S. Kobayashi and T. Yakou, Control of intermetallic compound layers at interface between steel and aluminum by diffusion-treatment, *Materials Science and Engineering*, A338 (2002) 44-53.
- [5] G. Sierra, P. Peyre, F. D. Beume, D. Stuart and G. Fras, Steel to aluminum key-hole laser welding, *Materials Science and Engineering*, A447 (2007) 197-208.
- [6] J. Sun, Q. Yan, W. Gao and J. Huang, Investigation of laser welding on butt joints of Al/steel dissimilar materials, *Materials & Design*, 83 (15) (2015) 120-128.
- [7] M. J. Torkamany, S. Tahamtan and J. Sabbaghzadeh, Dissimilar welding of carbon steel to 5754 aluminum alloy by ND;YAG Pulsed laser, *Materials & Design*, 31 (1) (2010) 458-465.
- [8] K. Martinsen, S. J. Hu and B. E. Carlson, Joining of dissimilar materials, *CIRP Annals - Manufacturing Technology*, 64 (2) (2015) 679-699.
- [9] M. Veral, A. Akkus and B. Eryurek, Effect of welding nugget diameter on the fatigue strength of the resistance spot welded joints of different steel sheets, *J. of Materials Processing Technology*, 176 (1-3) (2006) 127-132.
- [10] H. S. Choi, G. H. Park, W. S. Lim and B. M. Kim, Evaluation of weldability for resistance spot welded single-lap joint between GA780DP and hot-stamped 22MnB5 steel sheets, *JMST*, 25 (6) (2011) 1543-1550.
- [11] *ISO standard 18278-2:2004*, Resistance welding, Weldability, Part 2: Alternative procedures for the assessment of sheet steels for spot welding.
- [12] C.-W. Ji, I. Jo, H. Lee, I.-D. Choi, Y. D. Kim and Y.-D. Park, Effects of surface coating on weld growth of resistance spot-welded hot-stamped boron steels, *JMST*, 28 (11) (2014) 4761-4769.
- [13] S. Hassanifard and M. Feyzi, Analytical solution of temperature distribution in resistance spot welding, *JMST*, 29 (2) (2015) 777-784.
- [14] W. Zhang, D. Sun, L. Han and Y. Li, Optimized design of electrode morphology for novel dissimilar resistance spot welding of aluminum alloy and galvanized high strength steel, *J. of Materials and Design*, 85 (15) (2015) 461-470.
- [15] N. Muhammad, M. Hafidzi, S. K. Abas, G. Tham and E. Haruman, Optimization and modeling of spot welding parameters with simultaneous multiple response consideration using multi-objective Taguchi method and RSM, *JMST*, 26 (8) (2012) 2365-2370.



**Ji Sun Kim** is Junior Researcher in Department of Green Manufacturing process R&D group of KITECH. He received his M.S. degree from Mokpo National University. He has interested in welding engineering, dissimilar welding and optimizations of welding process.